Quantum many-body scars

Zhaohui Zhi

School of Physics, Beihang University; Faculty of Physics, TU Dresden

Jan 2024

Table of contents

The Rydberg atom arrays based quantum simulation platform

The Hamiltonian of the Rydberg atom arrays is:

$$\frac{H}{\hbar} = -\sum_{i=1}^{N} \Delta n_i + \sum_{<i,j>} \frac{V}{|d_i - d_j|^6} n_i n_j + \sum_{i=1}^{N} \Omega \sigma_i^x$$

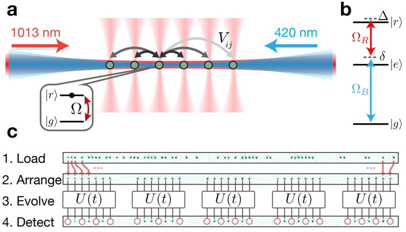

Figure: Experimental platform [1]

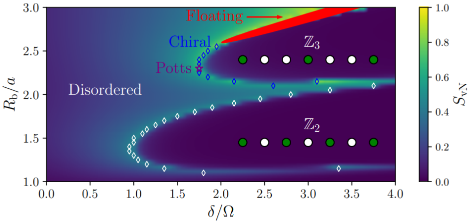

Figure: The phase diagram of 1D Rydberg atoms chain [8]

Promising quantum computation platform

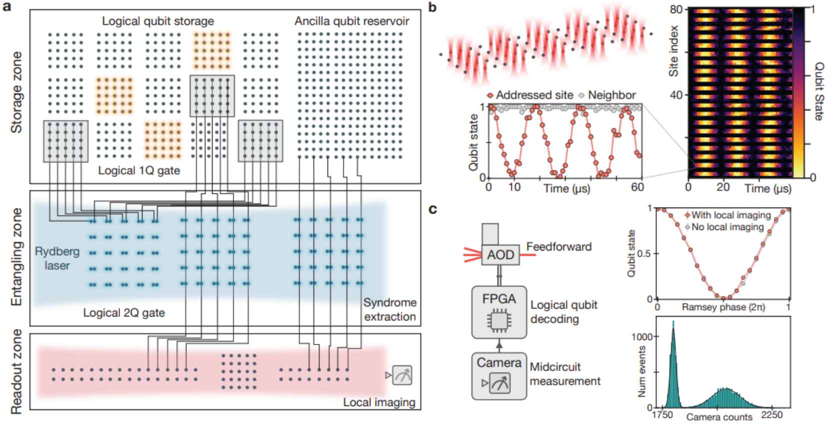

Figure: Logical quantum processor based on reconfigurable atom arrays [2]

A novel dynamics captured by Rydberg atom arrays experiments

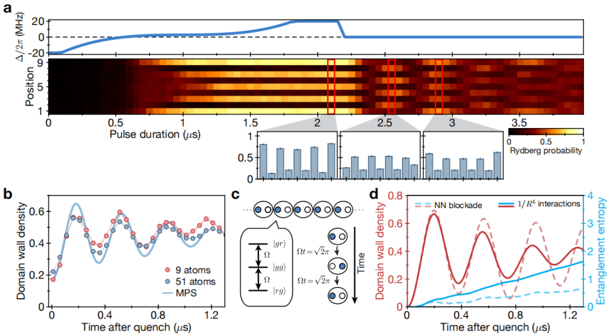

Figure: Emergent oscillations in many-body dynamics after sudden quench. [1]

Initial crystal state revivial with a frequency of $\Omega/1.38$ that is largely independent of the system size are observed. It behaves like non-interacting dimers model. MPS outcome and numerical calculations from ED support that.

Constrained model

After we turn off the laser quench the initial state and set $\Delta = 0$. Only consider strong N.N. interaction limit(small $\epsilon = \frac{\Omega}{V}$), we denote $V = V_{i,i+1}$:

$$H = \sum_i n_i n_{i+1} + \epsilon \sum_i X_i$$

then using the SW transformation, we introduce the low-energy subspace spanned by configurations with no adjacent excited states. The projector onto this subspace can be written as $P = \Pi_j (1 - n_i n_{i+1})$. The first non trivial term is $H_{\text{eff}} = \epsilon P \sum_i X P$. After removing overall scale ϵ, we obtain , where $P_i = 1 - n_i$

$$H_{\text{PXP}} = \sum_i P_{i-1} X_i P_{i+1} \tag{1}$$

Constrained model

The dim of such low-energy subspace after ruling out kinetically constrained states is a Fibonacci sequence [5]

$$\begin{cases} d_L^{OBC} = d_{L-1} + d_{L-2} \\ d_L^{PBC} = d_L + d_{L-4} \end{cases} \quad (2)$$

which mean, where F_l is Fibonacci sequence

$$\begin{cases} d_L^{OBC} = F_{L+2} \\ d_L^{PBC} = F_{L-1} + F_{L+1} \end{cases} \quad (3)$$

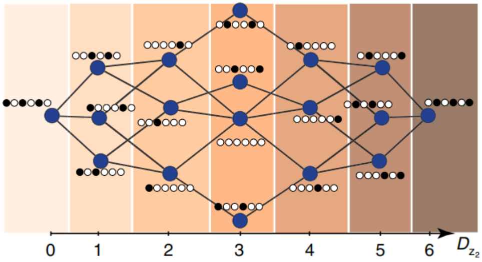

Figure: The constrained Hilbert space graph of the Fibonacci chain with L=6 sites over Hamming distance [7]

Symmetries for block diagonalization

The Exact Diagonalization need to consider the symmetry to block diagonalize.

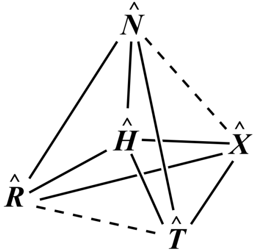

Figure: Commutation relations among the Hamiltonian and the symmetry operators. [6]

- Particle conservation symmetry: $N = \sum_i n_i, H = H_0 \oplus \cdots \oplus H_N \oplus \cdots \oplus H_L$
- Translational symmetry in PBC, $H_N = H_{N,0} \oplus \cdots \oplus H_{N,k} \oplus \cdots \oplus H_{N,L-1}$,build Representative State out of $|\bar{n}, k\rangle = \sum_{n=0}^{L-1} e^{\frac{i2\pi}{L}kn} T^n |\bar{n}\rangle$
- spatial inversion symmetry R which maps $i \to L - i + 1$. $R = R^\dagger$ where reflection operator defined as $RO_lR = O_{L-i-l}$.
- particle-hole symmetry $\mathcal{X} = \prod_i X_i$, but $[R, T] \neq 0, [N, X] \neq 0$

The Momentum sector and the maximum symmetry sector

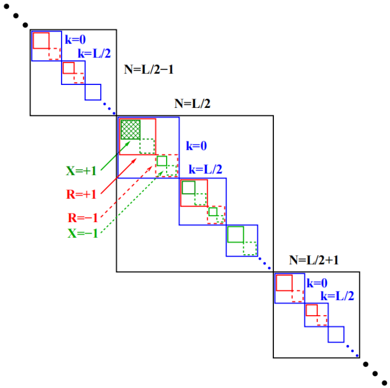

Figure: Block diagonal structure of the Hamiltonian matrix [6]

The discrete symmetry operators satisfy $X^{\dagger}(N-L/2)X=-(N-L/2)$.
In the half-filling sector $N=L/2$, (H,N,T,X) are mutually commuting.

$$H_{N=L/2,k}=H_{N=L/2,k,X=1}\oplus H_{N=L/2,k,X=-1}$$

And $R^{\dagger}TR^{-1}=T^{-1}$ means that at momentum sector $k=0,k=L/2$, $T=T^{-1}$, $[R,T]=0$.

$$H_{N,k}=H_{N,k,R=1}\oplus H_{N,k,R=-1}$$

So we focus on the maximum symmetry sector $S_{N=L/2,k=0,R=1,X=1}$

Symmetries of PXP model

Paticle-hole symmetry, $\{H_{\text{PXP}}, X\} = 0$, leads to each $|E\rangle$ has a partner $|-E\rangle$ in spectrum.
Then for PBC, we can explicitly evaluate the zero-momentum inversion-symmetric sector for different sites.

size	representatives/k=0	pure inversion	k=0,R=1 MSS
L=24	4341	377	2359
L=26	10462	610	5536
L=28	25415	987	13201
L=30	62075	1597	31836
L=32	152288	2584	77436

Table of contents

The consecutive level statistics

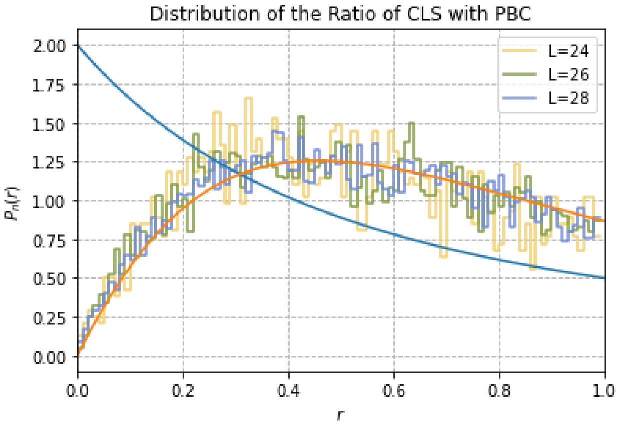

Figure: Level statistics and in the Fibonacci chain

Zero mode

The lower bound of zero-energy eigenstates in the zero-momentum sector [3]:

$$Z^0_{2l} \geq |Q^{(0,+)}_{2l} - Q^{(0,-)}_{2l}| = F_{l-1} \quad \text{PBC} \tag{4}$$

$$Z^0_{2l} \geq F_{l+1} \quad \text{OBC} \tag{5}$$

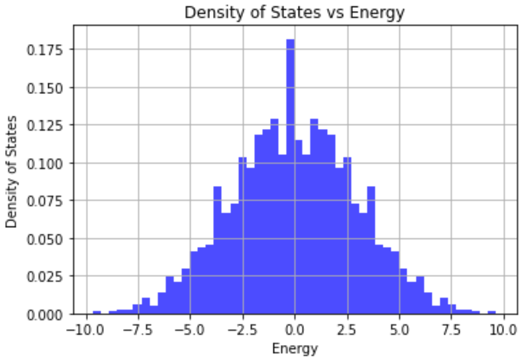

Figure: Density of states in PXP model and the zeros mode with L=28

Table of contents

Loschmit echo and entanglement entropy

we observe the special dynamics to calculate the Loschmit echo $|\langle \circ\bullet\circ\bullet\circ|e^{-\frac{iHt}{\hbar}}|\circ\bullet\circ\bullet\circ\bullet\rangle|^2$ and entropy curve $S = \mathrm{tr}(\rho \ln \rho)$ over time. And then compare different initial state

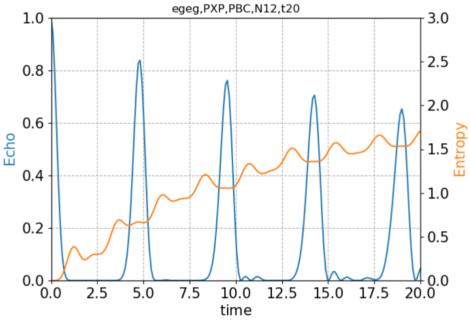

Figure: The Loschmit echo and the Von-Neumann entanglement entropy

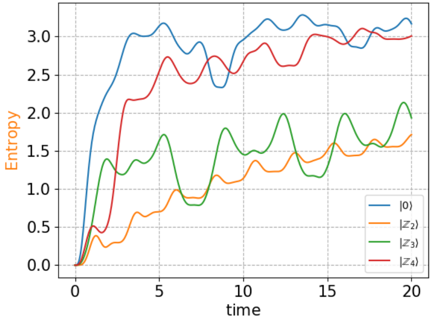

Figure: Entanglement entropy growth for different initial state $N = 24$ TDVP

Dynamics of entanglement and local correlation function

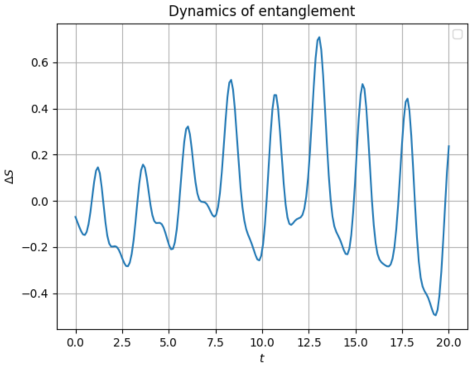

Figure: Dynamics of entanglement

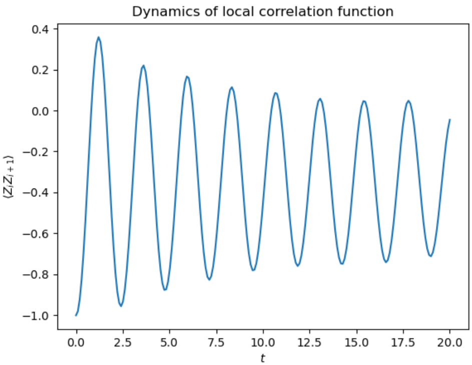

Figure: Dynamics of local correlation function

Table of contents

Overlap of states

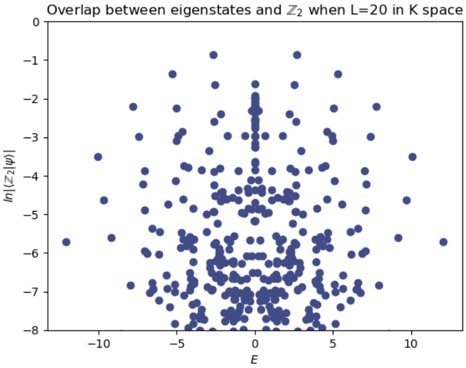

Figure: Overlap between eigenstates and $|\mathbb{Z}_2\rangle$, $L = 20$, in K space

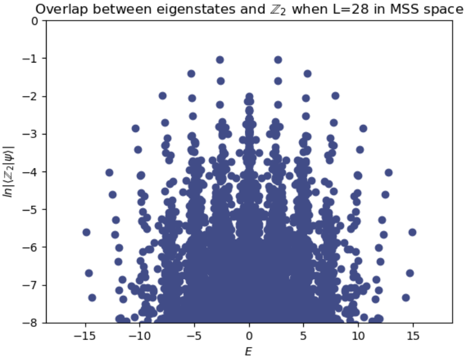

Figure: Overlap between eigenstates and $|\mathbb{Z}_2\rangle$, $L = 28$, in MSS space

Overlap of states

However, it's hard to identify many degenerate zero modes $|E=0\rangle$. We expect only one state in $\mathcal{H}_{\text{zero modes}}$ described by FSA state, i.e. we can use $P_{\text{zero modes}} P_{\text{FSA}} P_{\text{zero modes}}$, only one basis state with a non-zero overlap with $|\mathbb{Z}_2\rangle$.

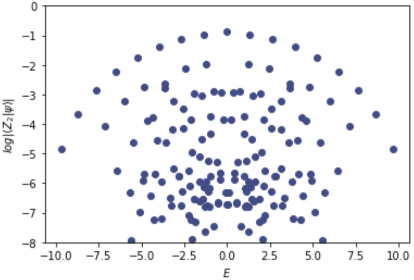

Figure: Overlap between eigenstates and $|\mathbb{Z}_2\rangle$, $L=16$, in constrained space, ruling out the degeneracy

FSA(Forward Scattering Approximation) and Emergent SU(2) symmetry [4]

Such special scar states can be spanned by FSA basis, $\{|\mathbb{Z}_2\rangle, H^+|\mathbb{Z}_2\rangle/b_1, (H^+)^2|\mathbb{Z}_2\rangle/b_2 \dots (H^+)^n|\mathbb{Z}_2\rangle/b_n\}$. where the $H^{\pm}$ is defined as:

$$H_{\pm} = \sum_{j\in\text{even}} P_{j-1}\sigma_j^{\pm}P_{j+1} + \sum_{j\in\text{odd}} P_{j-1}\sigma_j^{\mp}P_{j+1}$$

where $\beta_n = \langle n|H|n-1\rangle = \langle n+1|H|n\rangle$.And the z-projection of spin $H^z = \frac{1}{2}[H^+, H^-] = \sum_i^L(-1)^n\sigma_n^z/2$
Then $[H^z, H^{\pm}] \approx \pm H^{\pm}$, from which we can perceive the $SU(2)$ symmetry with a spin $L/2$ representation.

FSA and Emergent SU(2) symmetry [4]

Noting it only contains $L+1$ basis as the maximum Hamming distance is $L+1$, and in FSA basis, the PXP Hamiltonian be like:

$$H_{\text{FSA}} = \begin{pmatrix} 0 & \beta_1 & & & \\ \beta_1 & 0 & \beta_2 & & \\ & \beta_2 & 0 & \ddots & \\ & & \ddots & \ddots & \beta_L \\ & & & \beta_L & 0 \end{pmatrix}$$

$$\mathcal{H}_{\text{energyeigen}} = \mathcal{H}_{\text{FSA}} \oplus \mathcal{H}_{\text{thermal}}$$

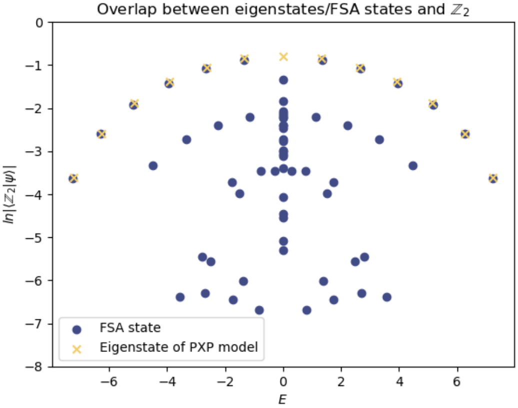

Figure: The FSA state and scar state in $L = 12$

FSA state and Exact state

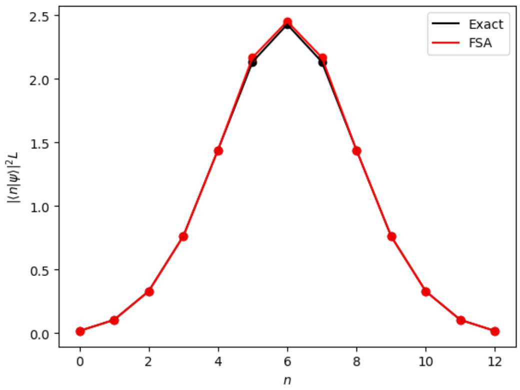

Figure: Overlap between FSA basis $|n\rangle$ and the FSA states(black) or the exact states(red)

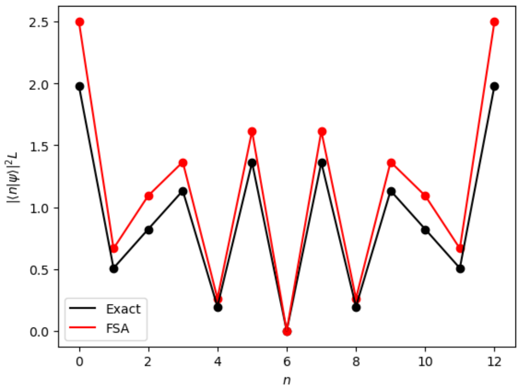

Figure: Overlap between FSA basis $|n\rangle$ and the FSA states(black) or the exact states(red)

Initial state with perturbation

These anomalous eigenstates ($O(L)$) are immersed in a much larger sea of thermal eigenstates($O(2^L)$), but underpin the real-time dynamics.

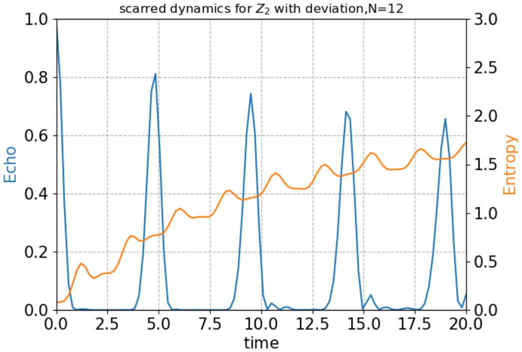

Figure: Scarrd dynamics with a deviation add to initial state

Table of contents

Reference I

Hannes Bernien, Sylvain Schwartz, Alexander Keesling, Harry Levine, Ahmed Omran, Hannes Pichler, Soonwon Choi, Alexander S. Zibrov, Manuel Endres, Markus Greiner, Vladan Vuletić, and Mikhail D. Lukin.
Probing many-body dynamics on a 51-atom quantum simulator.
Nature, 551(7682):579–584, nov 2017.

Dolev Bluvstein, Simon J. Evered, Alexandra A. Geim, Sophie H. Li, Hengyun Zhou, Tom Manovitz, Sepehr Ebadi, Madelyn Cain, Marcin Kalinowski, Dominik Hangleiter, J. Pablo Bonilla Ataides, Nishad Maskara, Iris Cong, Xun Gao, Pedro Sales Rodriguez, Thomas Karolyshyn, Giulia Semeghini, Michael J. Gullans, Markus Greiner, Vladan Vuletić, and Mikhail D. Lukin.
Logical quantum processor based on reconfigurable atom arrays.
Nature, December 2023.

Reference II

- Wouter Buijsman.
  Number of zero-energy eigenstates in the PXP model.
  Physical Review B, 106(4), jul 2022.

- Soonwon Choi, Christopher J. Turner, Hannes Pichler, Wen Wei Ho, Alexios A. Michailidis, Zlatko Papić, Maksym Serbyn, Mikhail D. Lukin, and Dmitry A. Abanin.
  Emergent su(2) dynamics and perfect quantum many-body scars.
  Phys. Rev. Lett., 122:220603, Jun 2019.

- Wen Wei Ho, Soonwon Choi, Hannes Pichler, and Mikhail D. Lukin.
  Periodic orbits, entanglement, and quantum many-body scars in constrained models: Matrix product state approach.
  Phys. Rev. Lett., 122:040603, Jan 2019.

Reference III

Jung-Hoon Jung and Jae Dong Noh.
Guide to exact diagonalization study of quantum thermalization.
Journal of the Korean Physical Society, 76(8):670–683, apr 2020.

Maksym Serbyn, Dmitry A. Abanin, and Zlatko Papić.
Quantum many-body scars and weak breaking of ergodicity.
Nature Physics, 17(6):675–685, may 2021.

Xue-Jia Yu, Sheng Yang, Jing-Bo Xu, and Limei Xu.
Fidelity susceptibility as a diagnostic of the commensurate-incommensurate transition: A revisit of the programmable rydberg chain.
Physical Review B, 106(16), oct 2022.